100% Internal Quantum Efficiency in Polychiral Single-Walled Carbon Nanotube Bulk Heterojunction/Silicon Solar Cells

Francesco De Nicola,[*,†,‡] Matteo Salvato,[†,fj] Carla Cirillo,[§,fj] Michele Crivellari,[‖] Maurizio Boscardin,[‖] Maurizio Passacantando,[⊥] Michele Nardone,[⊥] Fabio De Matteis,[#] Nunzio Motta,[‡] Maurizio De Crescenzi,[†] and Paola Castrucci[†]

[†]*Dipartimento di Fisica, Universitá di Roma Tor Vergata, Via della Ricerca Scientifica 1, 00133 Roma, Italy*

[‡]*Institute for Future Environments and School of Chemistry, Physics, and Mechanical Engineering, Queensland University of Technology (QUT), Brisbane 4001 QLD, Australia*

[fj]*CNR-SPIN Salerno, Universitá di Salerno, Via Giovanni Paolo II 132, 84084 Fisciano, Italy*

[§]*Dipartimento di Fisica, Universitá di Salerno, Via Giovanni Paolo II 132, 84084 Fisciano, Italy*

[‖]*Micro-nano Characterization and Fabrication Facility, Fondazione Bruno Kessler (FBK), Via Sommarive 18, 38123 Trento, Italy*

[⊥]*Dipartimento di Scienze Fisiche e Chimiche, Universit degli Studi dell'Aquila Via Vetoio, 67100 L'Aquila, Italy*

[#]*Dipartimento di Ingegneria Industriale, Universitá di Roma Tor Vergata, Via del Politecnico 1, 00133, Roma, Italy*

E-mail: fdenicola@roma2.infn.it

Abstract

Bulk heterojunction films made of polychiral single-walled carbon nanotubes (SWCNTs) form efficient heterojunction solar cells with n-type crystalline silicon (n-Si), due to their superior electronic, optical, and electrical properties. The SWCNT films are multi-functional, since their hierarchical surface morphology provides a biomimetical anti-reflective, air-stable, and hydrophobic encapsulation for Si. Also, the films have a large effective area conferring them high optical absorption, which actively contribute to the solar energy harvesting together with Si. Here, we report photovoltaic devices with photoconversion efficiency up to 12% and a record 100% internal quantum efficiency (IQE). Such unprecedented IQE value is truly remarkable and indicates that every absorbed photon from the device, at some wavelengths, generates a pair of separated charge carriers, which are collected at the electrodes. Furthermore, the SWCNT/Si devices favor high and broadband carrier photogeneration, extending the Si spectral response from the near infrared to the ultraviolet range; charge dissociation of ultra-fast hot excitons; transport of electrons through n-Si and high-mobility holes through the SWCNT percolative network. Moreover, by varying the SWCNT film thickness, it is possible tailoring physical properties of such a two-dimensional interacting system, therefore the overall device optoelectronic features. These results not only pave the way for low-cost, high-efficient, and broadband photovoltaics, but also they are promising for the development of generic

SWCNT-based optoelectronic applications.

Keywords

third generation solar cell; photovoltaic; bulk heterojunction; single-walled carbon nanotube; internal quantum efficiency; silicon; air-stable encapsulation; anti-reflective coating; hydrophobic film

Third generation photovoltaics require a combination of low-cost and highly efficient materials in order to overcome balance-of-system costs. Carbon nanotubes (CNTs) are particularly attractive for their earth-abundant source materials, recently scalable fabrication,[1] purification methods,[2] and solution processability. [3] Moreover, the unique one-dimensional properties of CNTs allow the realization of solar cells that are highly thermally conductive, mechanical, chemical, and radiation resistant.[4] In particular, single-walled carbon nanotubes (SWCNTs) have suitable photophysical properties[4] for photovoltaics, such as high aspect ratio, direct subband gaps,[5] and tunable photoabsorption from the near infrared (NIR) to the ultraviolet (UV) region.[2] Notably, SWCNT electronic and optical subband gaps are in a wide range: from 0.5 to 5 eV. Generally, one of the criteria for obtaining the highest photoconversion efficiency (PCE) is the correct matching of the solar cell band gap to the solar spectrum. The optimal device band gap of 1.1 eV[6] can be easily obtained with 12-15 different nanotube chirality having the first optical subband gap between 1.0-1.2 eV. Therefore, by using polychiral mixtures of both metallic and semiconducting SWCNTs it is possible having a broadband optical absorption throughout the UV-VIS-NIR range,[7] harvesting in this way the majority of the solar photon flux, meanwhile avoiding the time-consuming sorting process required to isolate single-chirality distributions of SWCNTs.[8] Furthermore, the photogenerated carriers in SWCNTs are excitons with binding energies up to 0.4 eV at room temperature, [9,10] which possibly may be multiple generated.[11,12] Consequently, such photogenerated excitons are ultra-fast transferred[13–15] through the SWCNT percolating network and they are dissociated into high-mobility (79000 cm^2/Vs)[16] free carriers in order to harvest their potential energy for solar cells and photodetectors. Such a dissociation is accomplished, for instance, by creating an heterojunction[17] with silicon (Si) due to the energetic band offsets greater than the SWCNT exciton binding energy.[18] In this way, charge generation, separation, transport, and collection can be realized partly by the semi-transparent, conductive SWCNT thin film and partly by Si. In addition, the large available surface area of the CNT random network films, provided by their multi-fractal hierarchical morphology,[3] leads to strong and tunable optical absorption,[7] anti-reflection,[19] and an air-stable,[20] hydrophobic encapsulation[3,50] for Si. For all these reasons, a deep understanding of polychiral SWCNT hierarchical random networks is critical in order to realize technologically relevant photovoltaic devices.

Carbon nanotube/silicon (CNT/Si) heterojunction solar cells have steadily pushed the PCE up to 12%[21] without any post-process treatments, while up to 11% for chemical doped cells,[22] 15% for integration with gold nanoparticles[8] or with anti-reflective coatings,[23] and a record 17%[24] exploiting oxide layers. Despite these accomplishments, our fundamental understanding of the SWCNT/Si heterojunctions is still incomplete.

Here, we report an unprecedented record 100% of internal quantum efficiency (IQE) for SWCNT/Si heterojunction solar cells. We also show for the first time that the multi-functional SWCNT film not only plays an active role in the heterojunction, but it also provides anti-reflection together with an air-stable and hydrophobic encapsulation for the solar cells. Furthermore, we introduce the SWCNT bulk heterojunction (BHJ), demonstrating that is an two-dimensional system formed by interacting SWCNTs. The optical and electrical properties of such a BHJ as well as those of the whole SWCNT/Si device are discussed. By independently optimizing the SWCNT film and Si thicknesses, we illustrate that it is possible tailoring in a controlled fashion the PCE of our

solar cells up to 12±1%. Finally, we suggest a detailed model for the SWCNT/Si heterojunction.

The SWCNT films were fabricated by a solution process and deposited by dry-transfer printing[3] on n^+-Si (100) substrates with Au/Cr patterned electrodes on SiO_2 [20] (see Supporting Information). The films appear as homogeneous and porous random networks of SWCNT bundles with a multi-fractal and hierarchical surface morphology,[3] as shown in Figure 1a,b. X-ray photoelectron spectroscopy (XPS) on our SWCNT films showed no trace of S or Na due to the SDS surfactant, within the experimental limit ≲1% of the technique. Also Raman spectroscopy reported an amount of defects as low as 12%. Therefore, the SWCNT films realized with our method are highly crystalline, pure, and surfactant-free (see Supporting Information).

The physical properties of SWCNTs provide a new dimension for solid state physics based on the great variety of possible geometries that are available for the nanotubes. Indeed, one of the most significant feature of SWCNTs is their one-dimensional electronic structure, which depends only on their characteristic dimension: the nanotube diameter. However, when SWCNTs are polydispersed and weaved into a macroscopic (≈ cm^2) but thin (≈ 10-100 nm) random network film, their individual physical properties are mixed and the whole system may be considered interacting and two-dimensional, due to its high aspect ratio (10^5-10^6). We show as follow that the characteristic dimension of this two-dimensional system is not the SWCNT diameter anymore, but the film thickness indeed.

In Figure 2a, absorption spectra of a SWCNT film and SWCNTs in liquid dispersion are shown. The main feature of the SWCNT absorbance spectra is the π-π^* surface plasmon resonance (SPR) at 250-300 nm.[25] Also, one-dimensional excitonic transitions are shown. By fitting the SWCNT absorbance spectrum in Figure 2b, we estimated 15 chirality in the range of the expected diameters 0.7-1 nm (see Supporting Information). Also, it is possible to relate the observed excitonic transitions to metallic (M_{11}, ≈ 10%) and semiconducting (S_{ii}, ≈ 90%) SWCNTs. Therefore, the realized films consist of polychiral semiconducting and metallic SWCNTs with diameters within 0.7-1 nm. In Figure 2a, a broadening and a redshift of the excitonic peaks in the SWCNT film spectrum, in comparison with the spectrum of SWCNTs in liquid dispersion, can be observed. This is due to the electronic interactions among the SWCNTs.[26] It is worth noting that the peak broadening is not due to aggregation or bundling of the SWCNTs, otherwise the SPR would also broaden,[27] which is not observed. The broadening of the excitonic peaks indicates the change from 1D-like to 2D-like transitions. Moreover, a 10 nm redshift toward long wavelength in the SPR, M_{11}, and S_{22} excitonic transitions can be ascribed to the change in refractive index from air (n = 1.0) to the aqueous solution with the SDS surfactant (n ≈ 1.3). However, a 50 nm redshift occurs for S_{11} transitions. Thus, a 40 nm redshift due not to the change in refractive index but to the SWCNT interactions occurs, which increase the absorption edge of the overall system by ≈ 300 meV. Therefore, the change from a one-dimensional system to an interacting two-dimensional system can be distinguished.[13,17,26] Furthermore, the absorbance $A(\lambda)$ of our SWCNT films scales as the Beer-Lambert law $A(\lambda) = \alpha(\lambda)\tau$, where $\alpha(\lambda)$ is the SWCNT random network absorption coefficient[7] (see Supplementary Information). Moreover, the absorption length $\delta(\lambda) = \alpha(\lambda)^{-1}$ for our SWCNT film compared with that of crystalline Si[6] is reported in Figure 2c. Unlike Si, which has an indirect band gap of 1.12 eV, SWCNTs efficiently and uniformly absorb light from NIR to UV, bearing a wide range of direct optical subband gaps matching the solar spectrum. Typically, a 300 μm thick Si wafer is required to absorb the incident light within 1000 nm. In turn, the SWCNT random network films possess an exceptionally high absorption coefficient, which means a very low absorption length. As shown in Figure 2c, just 24 nm thick SWCNT film is required to attenuate the incident light from the VIS to NIR range by a factor 1/e, a thickness about four orders of magnitude lower than Si. Such a high absorption is

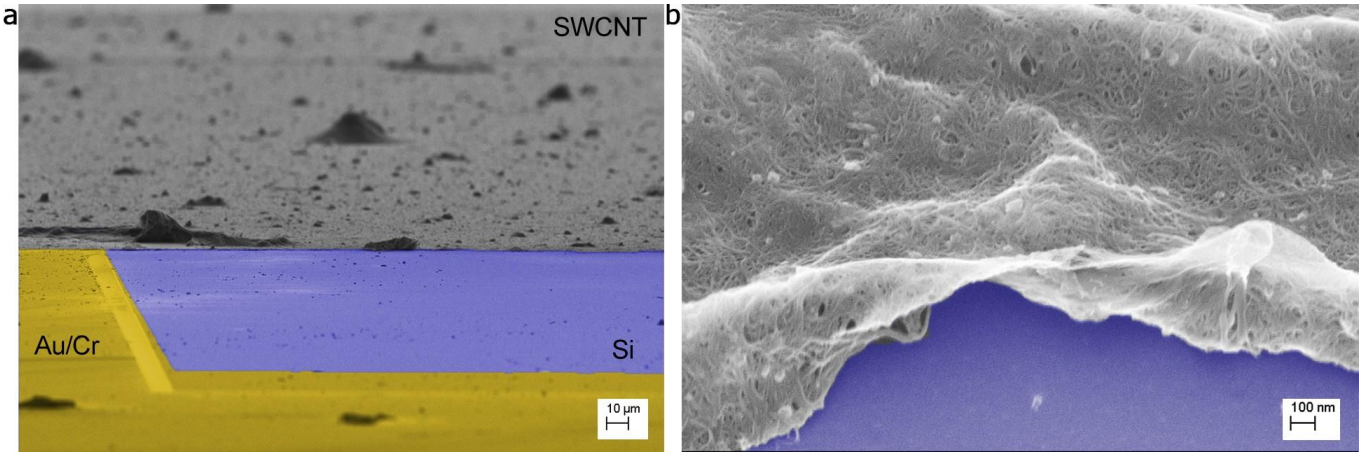

Figure 1: Scanning electron micrographs at tilted angle ($\approx 90^\circ$) of a SWCNT film deposited on the Si substrate of a solar cell. Magnification is 1k× (**a**) and 100k× (**b**). **a**, The SWCNT film, which is deposited on a Si (purple false color) substrate with Au/Cr patterned electrodes (yellow false color), appears to be homogeneous and defect-free. A microstructured roughness is also shown. **b**, At higher magnification, it is possible to observe that the microstructured roughness is made of a nanostructured SWCNT random network, thus realizing a two-fold hierarchical surface morphology.

due both to the SWCNT one-dimensional electronic properties and to their hierarchical surface morphology,[19] which provide them ultra-black properties.

In Figure 2d, the variation of the sheet resistance $R_{sh} = \rho/\tau$ with the SWCNT film thickness τ is shown. Since the sheet resistance is related to the film thickness by the SWCNT film resistivity ρ (Figure 2d), the thicker the film, the lower the sheet resistance, as well as the transmittance values (see Supplementary Information). Our SWCNT films may have low sheet resistance values with high transmittance, for instance a film 22.0 ± 0.5 nm thick has a transmittance T (550 nm) = 68% and a sheet resistance R_{sh} = 1 kΩ/*sq* (see Supplementary Information). From the fit in Figure 2d, we report for our SWCNT films $\rho = (2.5 \pm 0.4) \cdot 10^{-6}$ Ωm, in agreement with the resistivity of multi-walled carbon nanotube (MWCNT) films[20] and bulk graphite.[28]

The SWCNT film electrical conductance G as a function of its thickness τ is reported in Figure 2e. The plot shown in log scale follows the conductance percolation law[29] $G = G_0 (\tau_c - \tau)^{\mu}$, where G_0 is the conductance of the unity of the percolation network, the thickness τ_c is the conductance percolation threshold, μ is the universal (i.e. independent of the microscopic details of the system but scale dependent) critical exponent of percolation. The percolation law is valid when $\tau < \tau_c$ and $\tau_c - \tau$ is small. The plot states that as the SWCNT film thickness increases beyond the percolation threshold $\tau_c \approx 23$ nm, the conductance abruptly increases following the power law as conductive paths form. Conversely, below the percolation threshold the material is non-conducting. Fitting our data in log-log scale below the percolation threshold (Figure 2e, inset), we obtain $\mu = 1.27 \pm 0.11$, in agreement with the value reported for generic two-dimensional percolative systems ($\mu \approx 1.33$)[29] and MWCNT films.[20] Therefore, the percolation curve shows how to optimize the two-dimensional SWCNT film making it conductive with the lowest material amount.

Moreover, when semiconducting and metallic nanostructures are blended together, the overall electronic behavior resembles that of an amorphous metal.[18,30] Indeed, the electronic transport of the individual SWCNTs in the network is not purely ballistic anymore, nor quantum,[31] as it is rather dominated by disorder-induced hopping and non-resonant tunneling.[18,30] Additionally, an ultra-fast (0.2-10 ps) exciton energy transfer (EET) has been observed in SWCNT random network films.[13–15] In order to

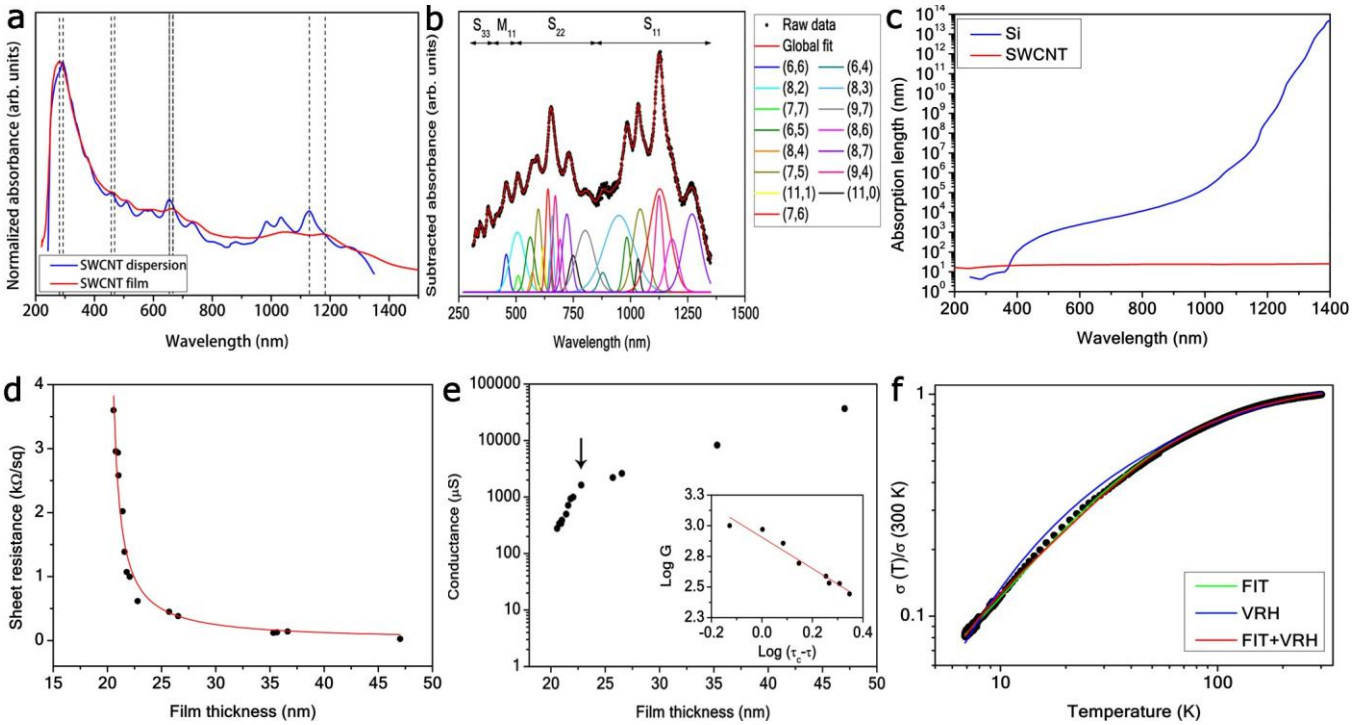

Figure 2: **a**, Absorbance spectra for SWCNTs dispersed in liquid and in a film. **b**, Assignment of the SWCNT chirality. Four regions can be identified for our SWCNTs in liquid dispersion: 300-400 nm (S_{33}), 400-550 nm (M_{11}), 550-900 nm (S_{22}), and 800-1350 nm (S_{11}), after subtracting the SPR tail by an exponential function. The convolution function (red solid line) of the individual Voigt functions (colored solid lines) fits the SPR-subtracted absorbance spectrum (black dots) in great agreement. **c**, Absorption length as a function of light wavelength for Si (blue solid line) and for our SWCNT films (red solid line). **d**, Sheet resistance as a function of SWCNT film thickness. **e**, Electrical conductance of the SWCNT films in log scale as a function of the film thickness. The black arrow marks the percolation threshold $\tau_c \approx$ 23 nm. The log-log plot of the conductance G as a function of the SWCNT film thickness in the inset is fitted by the conductance percolation law for $\tau < \tau_c$. **f**, Normalized conductivity of a 29 ± 1 nm thick SWCNT film as function of temperature. The plot is well fitted by a linear combination of VRH and FIT models.

investigate the conduction mechanism for our SWCNT films, we reported in Figure 2f the normalized conductivity $\sigma(T)/\sigma(300\ \mathrm{K})$ as a function of the temperature T for a SWCNT film with a thickness $\tau = 29 \pm 1$ nm, above the percolation threshold. The observed conductivity tends to zero as the temperature decreases, exhibiting a typical non-metallic behavior. We have been reported such a trend in conductivity also for MWCNT films,[20] and generally it has been observed for disordered metals or Fermi glasses, such as conjugated polymer films[18,30] and amorphous metals.[32] Usually, in those materials disorder and/or Coulomb interactions localize charge carriers at low temperature, inducing a metal/semiconductor transition. We fitted our data by the Mott's variable range hopping (VRH) transport[32] and the fluctuation-induced tunneling (FIT) transport.[33] However, the best fit is provided by the heterogeneous model,[20,29,30] which is a linear combination of the VRH and FIT models

$$\sigma(T) = c_1\sigma_0 e^{-(T_M/T)^{\gamma}} + c_2\sigma_t e^{[T_1/(T_0+T)]}. \quad (1)$$

From the fit of the curve $\sigma(T)/\sigma(300K)$ we obtain $\sigma_0 = 0.83 \pm 0.02$ the temperature-independent hopping conductivity, $T_M = 178 \pm 3$ K the Mott's characteristic temperature, $\sigma_t = 0.33 \pm 0.02$ the temperature-independent tunneling conductivity, $T_1 = 10 \pm 1$ K the activation temperature required for an electron to tunnel through an energy barrier, $T_0 = 0.4 \pm 0.5$

K the minimum temperature required to activate the thermal conduction to overcome the barrier, and $\gamma = 1/(d + 1) = 0.33 \pm 0.05$ the dimensionality dependent exponent. The fitted γ value suggests again that the system can be considered as two-dimensional ($d = 2$). Furthermore, c_1, c_2 are the normalized weights of the two transport models, which in our case state that 67% of the transport is by VRH and only 33% is by FIT. Therefore, our SWCNT films can be seen as disordered two-dimensional networks with large high-conductivity clusters separated by small low-conductivity clusters. In such a heterogeneous model, weakly localized electrons may percolate by thermally induced hopping between conducting regions, and tunnel through non-conducting regions. This description reasonably supports the fact that SWCNTs are randomly arranged with several intra- and inter-tube contacts, and local defects acting as electronic energy barriers, thus limiting the conduction. [20] Moreover, the presence of low-conductivity barrier clusters in the percolative path means that at frequencies above the semiconductor band gap the σ_{ac} will be greater than the σ_{dc}, as the former is determined by on-tube excitations and not by the inter-tube conductance. [29,30] Here, $\sigma_{ac}(550\ \text{nm})/\sigma_{dc} = 0.2$ (see Supplementary Information), which means that low-conductivity barrier clusters are negligible in the SWCNT films, and the optical excitations are not fixed on SWCNTs, but are mobile from tube to tube (i.e. EET).

A BHJ[18] is a solid state blend of nanoscale materials with different electronic structures. Typically, a BHJ has a microstructured morphology formed by spontaneous phase separation: the interfacial energy of BHJ components (donors and acceptors) favors high surface area, such that they self-assemble in order to form a microstructured and homogeneous interpenetrating network. Therefore, in a BHJ there is a donor-acceptor interface within a few nanometers, at any point of the space in the whole film volume. The optimization of such a particular morphology is required for efficient charge percolation in electronic devices. Since the exciton diffusion lengths and the carrier recombination lengths are typically on the order of tens of nanometers in nanomaterials such as SWCNTs,[34] the distance between the BHJ components must be approximately within this range and defects in the interpenetrating network must be avoided in order to not hamper the charge transport. Anyway, the morphology or the BHJ blend can be fine-tuned by controlling the solid-liquid phase separation during the film formation, by thermal annealing, or by varying the film thickness. In light of all the properties based on the experimental evidences illustrated so far for our SWCNT films, it is reasonable outlining the following considerations. Our self-assembled SWCNT films are a two-dimensional interacting system, which acts as a BHJ between the nanotubes. Despite the disordered nature of the junctions between the chirality involved in the film, a type-I heterojunction[13,17] may occur by the energy minimization principle, since charge carriers tend to propagate in regions of lower potential energy. Furthermore, when semiconducting and metallic SWCNTs are blended together the overall behavior resemble that of an amorphous metal. Also, depending on the BHJ electronic band structure, an ultra-fast EET may be achieved at the inter-tube interface throughout the SWCNT film volume, provided that the film conductivity percolation threshold has reached. Moreover, the hierarchical morphology of our SWCNT films, which mimic that of natural surfaces, provides a large accessible surface area that enables to tailor their optical properties, allowing an efficient and broadband light absorption within the thin material thickness.

Sketches of the SWCNT/Si solar cells are shown in Figure 3a. Despite the accomplishments in realizing SWCNT/Si solar cells, the fundamental understanding of these heterojunctions is still incomplete. Indeed, there is a strong disagreement in the scientific community on whether SWCNT/Si devices represent Schottky, metal-insulator-semiconductor (MIS), or p-n heterojunctions.[35] However, those models cannot accurately describe the complex SWCNT/Si system. In Figure 3b, a detailed band scheme for our SWCNT/Si heterojunction is depicted. The problem may be

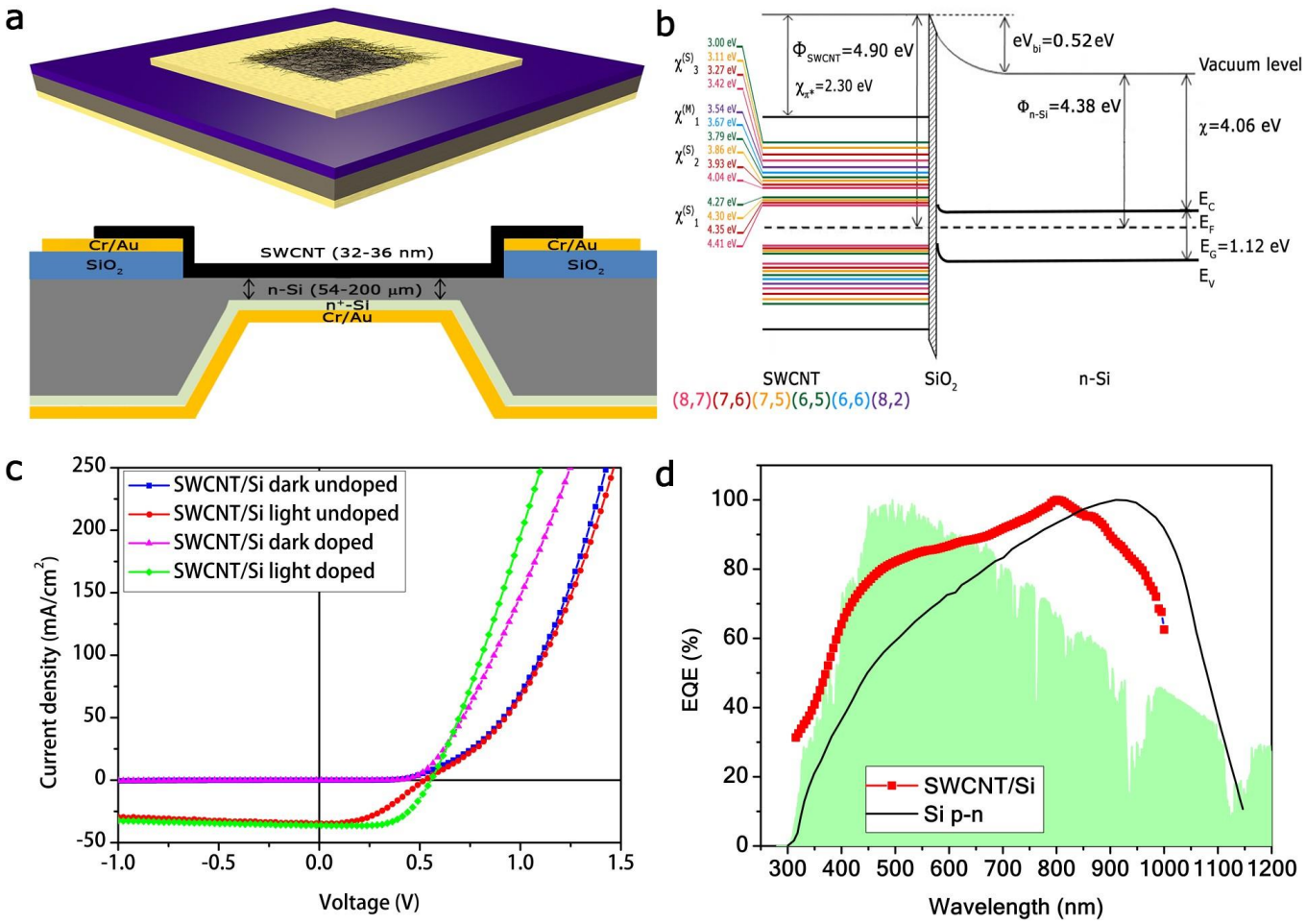

Figure 3: **a**, Three-dimensional and cross-sectional sketches of the SWCNT/Si solar cell. **b**, Energetic band scheme of the SWCNT/Si heterojunction in reverse polarization ($V < 0$). **c**, Electrical response of the best SWCNT/Si device before doping under dark (blue dotted line) and under illumination (red dotted line), and after doping under dark (magenta dotted line) and under illumination (green dotted line). **d**, External quantum efficiency of our best device (red dotted line) in comparison with that of a reference p-n Si solar cell (black solid line) and the AM 1.5 G solar irradiance spectrum (green shaded area). Spectra are normalized to the maximum value.

separated considering first the SWCNT film BHJ and then the SWCNT/Si heterojunction. As aforementioned, all the chirality assigned in our polychiral SWCNT film form a BHJ. Let us consider for simplicity only the dominant chirality (8,7), (7,6), (7,5), (6,5), (6,6), (8,2), whose absorbance is higher. Assume then that the SWCNTs are electronically intrinsic. The energy levels have been adjusted in relation to the vacuum level and equilibrated at the Fermi energy. Since the largest SWCNT diameter is $\approx$ 1 nm, each chirality has approximately the same work function $\Phi_{SWCNT} \approx$ 4.90 eV,[36,37] but different electron affinity levels and subband gaps. In particular, in the UV-VIS-NIR range investigated five electron affinity levels $\chi_i^{(S)}$ can be distinguished for the considered SWCNT chirality: three for the S_1, S_2, and S_3 conduction subbands of the semiconducting SWCNTs, a $\chi_1^{(M)}$ for the M_1 conduction subband of the metallic SWCNTs, and a $\chi_{\pi*}$ for the π^* subband, which is present in every chirality. Interestingly, although the S_1, S_2, and S_3 subbands for a given semiconducting chirality are well separated in energy by an extent higher than the thermal energy (k_BT = 25 meV), the three subbands of every considered chirality are close in energy. This reflects in the formation of three well-spaced conduction and valence narrow minibands. Moreover, the

M_1 subbands of metallic chirality fill the gap between the S_2 and S_3 narrow minibands. The fact that each subband is still separated from another by an energy higher than the thermal energy means that the subbands are uncoupled by a single thermal phonon and possess their own quasi-Fermi levels.[6]

On the other hand, the band gap E_G and the work function Φ_{Si} of the intrinsic Si are about 1.12 eV and 4.62 eV, respectively. The conduction band position in energy of our n-Si is denoted by its electron affinity χ = 4.06 eV, thus the valence band lies at 5.17 eV. In our case, for a dopant concentration of $N_D \cong 6 \cdot 10^{14}$ cm^{-3} the quasi-Fermi level is 0.32 eV below the conduction band, therefore our n-Si work function is Φ_{n-Si} = 4.38 eV. When n-Si is adjoined to the SWCNT BHJ, a type-II or staggered heterojunction between the SWCNT chirality with the smallest subband gap (0.98 eV) and Si takes place,[38,39] with a built-in potential (*i.e.* the difference $\Delta\Phi$ between the Si and SWCNT work functions) $eV_{bi} = \Delta\Phi$ = 0.52 eV. The maximum spatial band bending of Si for V = 0 is about 4 μm. The difference in Fermi levels and electronic affinity between the SWCNT and Si leads to singularities at the junction, which favor the electron transport, while constitute a barrier for the hole transport.[17] However these singularities are removed by the formation of the thin SiO_2 layer, which acts also as a spacer. Since the SWCNT/Si heterojunction Fermi level can be fine tuned by chemical doping, it is not pinned by SWCNT metallic subbands. Therefore, this kind of heterojunction cannot be considered just as a Schottky, nor as a p-n, or as a MIS heterojunction. It is worth noting that in SWCNT/Si solar cells the photogeneration occurs both in the Si and SWCNT films. Moreover, charge separation of photogenerated excitons in the SWCNT film occur due to the large built-in field at the interface between SWCNT films and Si. In particular, in reverse polarization ($V < 0$) hot electrons[14] photogenerated in the SWCNTs are ultra-fast transferred to the n-Si region, while hot holes are transported with high mobility[16] to the Au/Cr electrode through the SWCNT percolative network.

We report in Figure 3c the electrical response of the best SWCNT/Si (32 nm/200 μm) device in the dark state and under illumination (light state), before and after chemical doping by HNO_3 vapors for 10 s. For the undoped device, we achieved a PCE = 8 $\pm$ 1%, with a fill factor FF = 42 $\pm$7%. From the analysis of the light state curve (see Supplementary Information), we extrapolated the short circuit current density J_{sc} = 34.4 $\pm$ 0.1 mA/cm^2 and the open circuit voltage V_{oc} = 0.52 $\pm$ 0.01 V, while analyzing the dark state curve we obtained the reverse saturation current density J_0 = 5.21 $\pm$0.01 10^{-4} mA/cm^2, the shunt resistance R_p = 353 $\pm$1 MΩ/cm^2, the series resistance R_s = 144 $\pm$2 Ω/cm^2), and the diode ideality factor n = 1.32 $\pm$0.01. The extremely high shunt resistance value together with the very low value of reverse saturation current density and series resistance lead to such a high value of PCE, for this kind of devices. Furthermore, n is very close to the ideal value. On the other hand, for the doped device we achieved a 50% relative increment of the FF from 42 $\pm$ 7% to 63 $\pm$ 7%, therefore the PCE from 8 $\pm$ 1% to 12 $\pm$1% (Figure 3c). Interestingly, after doping the dark and light state curves intersect each others, and the light state curve present a negative differential resistance in reverse polarization. These two features are respectively hints of a higher recombination rate,[40] and the degenerate nature[41] of the SWCNT films after doping (see Supplementary Information).

In addition, the experimental external quantum efficiency (EQE) spectrum for our best SWCNT/Si (32 nm/200 μm) solar cell in comparison with a p-n Si reference cell (Minolta AK200), together with the AM 1.5 G solar spectrum are reported in Figure 3d. Spectra are normalized to the maximum value in order to highlight differences in the two devices. It is evident from the plot that our SWCNT/Si cell has a higher efficiency in the VIS range, within one standard deviation from the solar spectrum peak. Furthermore, the SWCNT/Si heterojunction has a larger spectral interval of efficiency than the p-n Si cell, ranging from UV to VIS. Also, a large EQE contribution in the NIR above the Si band gap due to the SWCNT

absorption is expected, as it has been reported by other authors.[42] We can thus infer that the SWCNT/Si solar cells are very promising devices for third generation photovoltaics, with a high and broadband efficiency.

Such an efficiency can be optimized by tailoring the SWCNT film processing and device post-treatments, as we reported for MWCNT/Si devices.[20] Here, the performance of our devices was optimized by independently fine tuning the SWCNT film and Si wafer thicknesses. We report the experimental solar cell electrical response under illumination and the EQE as a function of the SWCNT film thickness for a cell with 200 μm thick Si wafer (Figure 4a-c), and as a function of the Si wafer thickness for a cell with 32 ± 5 nm thick SWCNT film (in Figure 4b-d). We can infer from data that the SWCNT/Si (32 nm/200 μm) device configuration is the best, since it has both the highest PCE and EQE. It is worth noting the large variation across the full range of the EQE as a function of the SWCNT film thickness (Figure 4c), in comparison with the small EQE variation as a function of the Si wafer thickness (Figure 4d). In particular, the change in the Si wafer thickness affects more the EQE at long wavelengths, where the recombination effects at the back of the device compete with the higher absorption efficiency. Indeed, these recombination effects are expected for wafers thicker than the electron diffusion length. On the other hand, the thickness change in the SWCNT films dramatically affects the whole EQE spectrum. We remark that the SWCNT exciton diffusion length has been reported to be 6-90 nm,[34] consistent with our best SWCNT film thickness observed. Moreover, a film thickness of 32 ± 5 nm is beyond the aforementioned conductance percolation threshold and absorption length, therefore the SWCNT film is well conducting and can efficiently absorb light and transport the photogenerated minority carriers through the percolative network, in order to collect them at the electrodes.

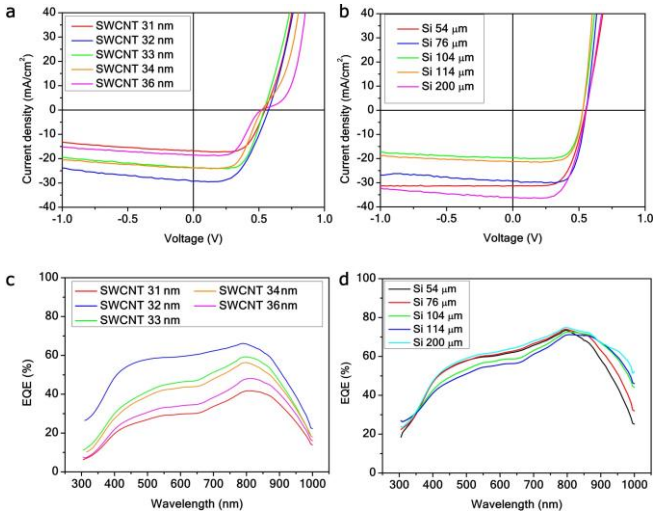

Figure 4: Electrical response (**a**) and EQE (**b**) of the SWCNT/Si solar cell as a function of the SWCNT film thickness for a cell with 200 μm thick Si wafer. Electrical response (**c**) and EQE (d) of the SWCNT/Si solar cell as a function of the Si wafer film thickness for a cell with 32 ± 5 nm thick SWCNT film.

One of the primary obstacles in realizing practical applications is the poor operational lifetime of the CNT/Si devices. Most inorganic and especially organic semiconducting materials degrade when exposed to moisture and/or oxygen. Also, photo-oxidation can be a serious problem. The degradation of devices made of such materials can be eliminated, or at least reduced to acceptable levels, by sealing the components inside an impermeable package using polymers,[43–45] oxides,[23] or metals.[6] Although such encapsulation methods can prevent or at least reduce oxygen and moisture permeation, they complicate the fabrication process, also resulting in increased thickness, shaded active surface, and loss of flexibility. Typically, encapsulation is responsible for 30-40% of the material and manufacturing total costs per Wp.[46] Thus, the realization of novel methods for enhancing device lifetime is an important goal that must be accomplished without interfering with the principal device concepts. This can be achieved by enabling clean and simple device fabrication by solution processing, keeping the device flexibility and thin form factor. Since CNTs are chemically stable, the device degradation typically comes from the Si detrimental oxidation in air.[47] Recently, CNT/Si air-stable devices up to a month have been reported with[21] and without[8,20] further encap-

sulation.

It can be observed in Figure 5a that the PCE of our devices is fairly stable after several weeks, although they are not encapsulated. In particular, our solar cells reach a maximum of PCE after approximately three days. This fact is due to the formation of an optimal thin Si oxide layer (1-2 nm) at the CNT/Si interface.[20,47] Differently by other CNT/Si devices reported,[21,22,43,45,48,49] the PCE of our solar cell does not degrade with time because of Si oxidation. Actually, the cell is stable after the oxide growth saturates (See Supplementary Information).

We previously reported on the wetting properties of hierarchical SWCNT coatings.[3,50] As shown in Figure 5b, the solar cell Si substrate result hydrophobic after the coating by a SWCNT film, due to the petal effect, achieving a quite stable[3] contact angle value $\vartheta = 110 \pm 3^\circ$, which is comparable to that of commercial hydrophobic polymers such as polydimethylsiloxane (PDMS, $\vartheta \approx 110^\circ$), currently used as encapsulating layers.

Anti-reflective coatings made of polymers or oxides have been employed to suppress the Si optical reflection in CNT/Si solar cells,[23,43–45] hence increasing their EQE. However, those films are not broadband, being quarter-wavelength coatings, and they require a further fabrication step. We have been recently investigated the anti-reflective properties of SWCNT hierarchical random network films.[19] In particular, their hierarchical surface morphology is able to suppress the Si optical reflection over a broad range of wavelengths, angles of incidence, and for both polarizations of light, by exploiting the moth-eye effect. Here, we show for the first time that the anti-reflective properties of these SWCNT films can be exploited for photovoltaic applications, without the need of further coatings.

In Figure 5c the total and diffuse reflectance are reported for SWCNT/Si solar cells with different SWCNT film thicknesses, and for a bare Si substrate as a control sample. It is possible to observe that the SWCNT films act as broadband anti-reflective coatings for Si. For instance, the high total reflectance of Si (27-70%) in the UV-VIS-NIR range investigated can be reduced down to 14-33% by a SWCNT film as thin as 32 ± 5 nm. In Figure 5c, it is also shown that the SWCNT coatings do not vary the Si diffuse reflectance (3-10%). Although the film surface roughness is quite high (Figure 1b), the SWCNT coatings do not behave as random scatterer surfaces, which are known to efficiently trap light inside the device.[6] Therefore, the most of the sample reflectance is specular and the anti-reflective behavior is only due to the moth-eye effect. Moreover, for the conservation of the energy $A + R + T = 1$. Since the solar cell is bulk with a reflective Au/Cr back electrode, its transmittance is $T \approx 0$. The total absorbance $A = 1 - R$ of our best solar cell is reported in Figure 5d, along with the total absorbance of the SWCNT film $A_{SWCNT} = 1 - R_{SWCNT} - T_{SWCNT}$, $R_{SWCNT} \approx 0 - 4\%$ and the Si wafer $A_{Si} = 1 - R_{SWCNT-Si} - T_{SWCNT} - T_{Si}$ (see Supplementary Information). Thus, the light that is not reflected is partly absorbed by the SWCNT film, and partly by the Si underneath. Although the absorption coefficient of hierarchical SWCNT random networks is higher than that of Si, the Si wafer thickness is such that it absorbs the most of the incoming light. Additionally, we estimated by the quantity $(A_{Si} + A_{SWCNT} - A)/(A_{Si} + A_{SWCNT})$ a 20% absorption losses in the solar cell. Furthermore, the internal quantum efficiency (IQE) of our best device is shown in Figure 5e along its EQE and the total reflectance (R). We achieved a 100% record IQE in the range 795-875 nm. Such a high IQE value is truly remarkable and indicates that every absorbed photon at these wavelengths generates a pair of separated charge carriers, and they are all collected at the electrodes.

In summary, our results represent a proof-of-concept of solar cells with high efficiency and reduced cost, by integrating SWCNTs with Si. For instance, about 32 nm thick SWCNT film made of 46 μg of SWCNTs, and only 200 μm of crystalline Si are needed to make a heterojunction solar cell with PCE up to $12 \pm 1\%$ and a EQE up to 70%. In this way, a reduction of Si about 150% with respect to conventional Si p-n solar cells has been obtained for our efficient de-

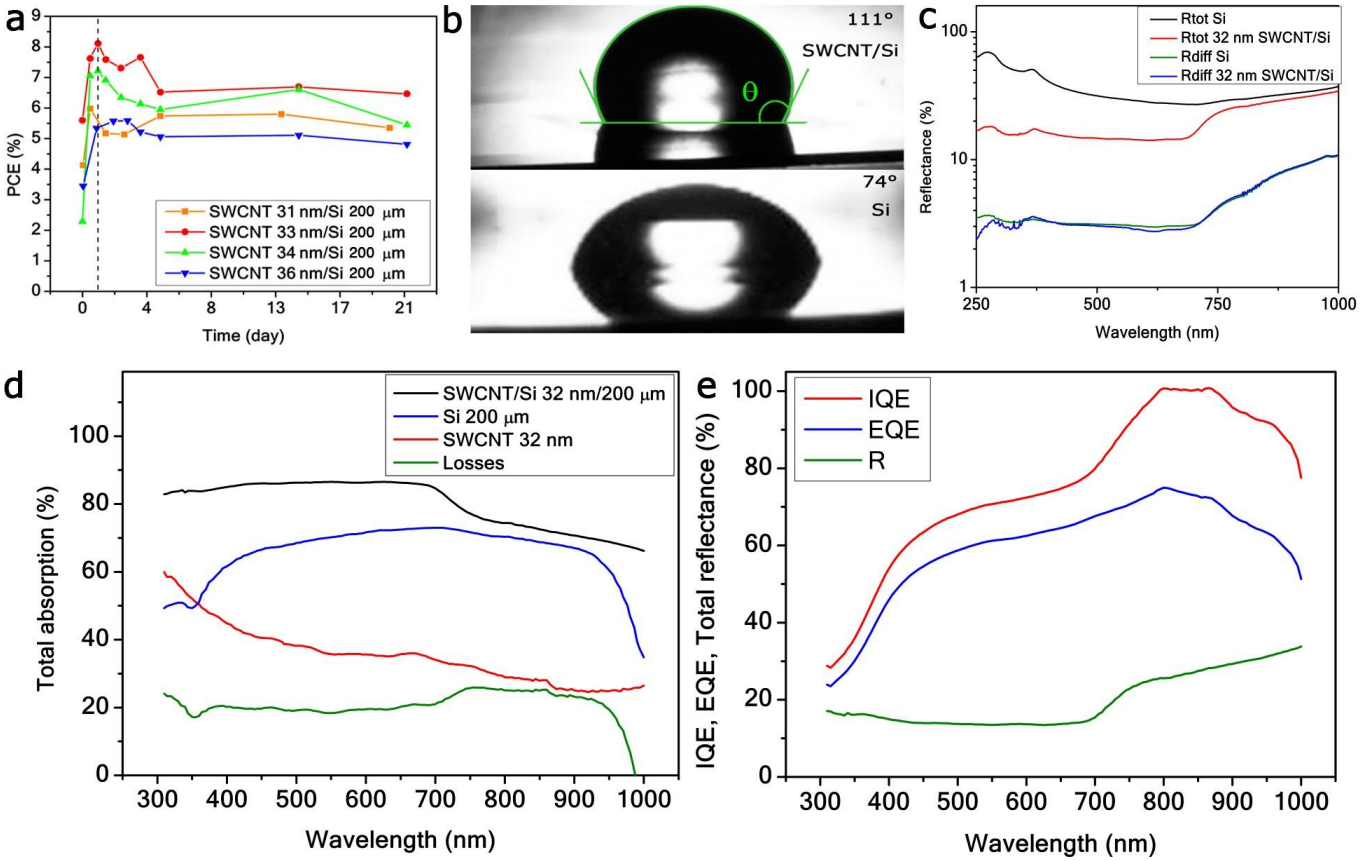

Figure 5: **a**, Photoconversion efficiency of several devices with different SWCNT/Si thickness configurations as a function of the elapsed time. **b**, Water droplets cast on a SWCNT/Si solar cell and on a solar cell Si substrate, as a reference. **c**, Total (red solid line) and diffuse (blue solid line) reflectance of SWCNT/Si solar cells with 32±5 nm thick SWCNT film. As a control sample, the total (black solid line) and diffuse (green solid line) reflectance of a bare Si substrate is also reported. **d** Total absorption of our best SWCNT/Si (32 nm/200 μm) solar cell (black solid line), of the SWCNT film 32 nm thick (red solid line), and of the Si substrate 200 μm (blue solid line). Absorption losses (green solid line). **e**, Comparison among EQE, IQE, and R of our best SWCNT/Si (32 nm/200 μm) solar cell.

vices. Also, the multi-functional SWCNT film form a BHJ that provides exceptional electrical and electronic properties, high and broadband absorption, together with an anti-reflective, hydrophobic, and air-stable encapsulation. Although, our results are comparable to the best PCE values of SWCNT/Si photovoltaic cells reported by other authors (without any post-process treatments and after chemical doping), our devices further achieve a record 100% IQE at some wavelengths.

Acknowledgement The authors acknowledge the support of the Australian Research Council (ARC) through the Discovery project DP130102120. F.D.N. gratefully acknowledges QUT for financial support. Part of the data reported in this paper were obtained at the Central Analytical Research Facility operated by the Institute for Future Environments (QUT). Access to CARF is supported by generous funding from the Science and Engineering Faculty (QUT). We thank the European Community for the RISE Project CoExAN GA644076.

The authors declare no competing financial interests.

References

(1) Hata, K.; Futaba, D. N.; Mizuno, K.; Namai, T.; Yumura, M.; Iijima, S. *Science* **2004**, *306*, 1362–1364.

(2) Arnold, M. S.; Green, A. A.; Hulvat, J. F.; Stupp, S. I.; Hersam, M. C. *Nat. Nanotechnol.* **2006**, *1*, 60–65.

(3) De Nicola, F.; Castrucci, P.; Scarselli, M.; Nanni, F.; Cacciotti, I.; De Crescenzi, M. *Sci. Rep.* **2015**, *5*, 1–9.

(4) Jorio, A.; Dresselhaus, G.; Dresselhaus, M. S. *Carbon Nanotubes Advanced Topics in the Synthesis, Structure, Properties and Applications*; Springer: New York, 2008.

(5) Saito, R.; Dresselhaus, G.; Dresselhaus, M. S. *Physical Properties of Carbon Nanotubes*; Imperial College Press: London, 1998.

(6) Nelson, J. *The Physics of Solar Cells*; Imperial College Press: London, 2003.

(7) De Nicola, F.; Pintossi, C.; Nanni, F.; Cacciotti, I.; Scarselli, M.; Drera, G.; Pagliara, S.; Sangaletti, L.; De Crescenzi, M.; Castrucci, P. *Carbon* **2015**, *95*, 28–33.

(8) Harris, J. M.; Semler, M. R.; May, S.; Fagan, J. A.; Hobbie, E. K. *J. Phys. Chem. C* **2015**, *119*, 10295–10303.

(9) Wang, F.; Dukovic, G.; Brus, L. E.; Heinz, T. F. *Science* **2005**, *308*, 838–841.

(10) Wang, F.; Cho, D. J.; Kessler, B.; Deslippe, J.; Schuck, P. J.; Louie, S. G.; Zettl, A.; Heinz, T. F.; Shen, Y. R. *Phys. Rev. Lett.* **2007**, *99*, 2274011–2274014.

(11) Wang, S.; Khafizov, M.; Tu, X.; Zheng, M.; Krauss, T. D. *Nano Lett.* **2010**, *10*, 2381–2386.

(12) Gabor, N. M.; Zhong, Z.; Bosnick, K.; Park, J.; McEuen, P. L. *Science* **2009**, *325*, 1367–1371.

(13) Mehlenbacher, R. D.; McDonough, T. J.; Grechko, M.; Wu, M.-Y.; Arnold, M. S.; Zanni, M. T. *Nat. Commun.* **2015**, *6*, 6732–6739.

(14) Ponzoni, S.; Galimberti, G.; Sangaletti, L.; Castrucci, P.; Gobbo, S. D.; Morbidoni, M.; Scarselli, M.; Pagliara, S. *J. Phys. Chem. C* **2014**, *118*, 2411024116.

(15) Grechko, M.; Ye, Y.; Mehlenbacher, R. D.; McDonough, T. J.; Wu, M.-Y.; Jacobberger, R. M.; Arnold, M. S.; Zanni, M. T. *ACS Nano* **2014**, *8*, 5383–5394.

(16) Dürkop, T.; Getty, S. A.; Cobas, E.; Fuhrer, M. S. *Nano Lett.* **2004**, *4*, 35–39.

(17) Davies, J. H. *The Physics of Low-Dimensional Semiconductors An Introduction*; Cambridge University Press: Cambridge, 1998.

(18) Heeger, A. J.; Sariciftci, N. S.; Namdas, E. B. *Semiconducting and Metallc Polymers*; Oxford University Press: Oxford, 2010.

(19) De Nicola, F.; Hines, P.; De Crescenzi, M.; Motta, N. *Carbon* **2016**, *108*, 262–267.

(20) De Nicola, F.; Salvato, M.; Cirillo, C.; Crivellari, M.; Boscardin, M.; Scarselli, M.; Nanni, F.; Cacciotti, I.; De Crescenzi, M.; Castrucci, P. *Carbon* **2016**, *101*, 226–234.

(21) Wang, F.; Kozawa, D.; Miyauchi, Y.; Hiraoka, K.; Mouri, S.; Ohno, Y.; Matsuda, K. *ACS Photonics* **2014**, *1*, 360–364.

(22) Jia, Y.; Cao, A.; Bai, X.; Li, Z.; Zhang, L.; Guo, N.; Wei, J.; Wang, K.; Zhu, H.; Wu, D.; Ajayan, P. M. *Nano Lett.* **2011**, *11*, 1901–1905.

(23) Shi, E.; Zhang, L.; Li, Z.; Li, P.; Shang, Y.; Jia, Y.; Wei, J.; Wang, K.; Zhu, H.; Wu, D.; Zhang, S.; Cao, A. *Sci. Rep.* **2012**, *2*, 1–5.

(24) Wang, F.; Kozawa, D.; Miyauchi, Y.; Hiraoka, K.; Mouri, S.; Ohno, Y.; Matsuda, K. *Nat. Commun.* **2015**, *6*, 6305–6312.

(25) Murakami, Y.; Einarsson, E.; Edamura, T.; Maruyama, S. *Phys. Rev. Lett.* **2005**, *94*, 0874021–0874024.

(26) Grahn, H. T. *Semiconductor Superlattices: Growth and Electronic Properties*; World Scientific: Singapore, 1995.

(27) Kumar, C. S. S. R. *UV-VIS and Photoluminescence spectroscopy for nanomaterials characterization*; Springer: New York, 2013.

(28) Wallace, P. R. *Phys. Rev.* **1947**, *71* .

(29) Sahimi, M. *Applications of Percolation Theory*; CRC Press: Boca Raton, 2009.

(30) Kaiser, A. B. *Rep. Prog. Phys.* **2001**, *64*, 1–49.

(31) Dekker, C. *Physics today* **1999**, *52*, 22–28.

(32) Mott, N. F. *Adv. Phys.* **1967**, *16*, 49–144.

(33) Sheng, P. *Phys. Rev. B* **1980**, *21*, 2180–2195.

(34) Lüer, L.; Hoseinkhani, S.; Polli, D.; Crochet, J.; Hertel, T. *Nat. Physics* **2009**, *5*, 54–58.

(35) Tune, D. D.; Flavel, B. S.; Krupke, R.; Shapter, J. G. *Adv. Energy Mater.* **2012**, *2*, 1043–1055.

(36) Su, W. S.; Leung, T. C.; Chan, C. T. *Phys. Rev. B* **2007**, *76*, 2354131–2354138.

(37) Shiraishi, M.; Ata, M. *Carbon* **2001**, *39*, 19131917.

(38) Gong, M.; Shastry, T. A.; Xie, Y.; Bernardi, M.; Jasion, D.; Luck, K. A.; Marks, T. J.; Grossman, J. C.; Ren, S.; Hersam, M. C. *Nano Lett.* **2014**, *14*, 5308–5314.

(39) Landi, B. J.; Castro, S. L.; Ruf, H. J.; Evans, C. M.; Bailey, S. G.; Raffaelle, R. P. *Sol. Energy Mater. Sol. Cells* **2005**, *87*, 733–746.

(40) Nelson, J.; Kirkpatrick, J.; Ravirajan, P. *Phys. Rev. B* **2004**, *69*, 0353371–03533711.

(41) Sze, S. M. *Physics of Semiconductor devices*; John Wiley & Sons: New York, 1969.

(42) Lehman, J.; Sanders, A.; Hanssen, L.; Wilthan, B.; Zeng, J.; Jensen, C. *Nano Lett.* **2010**, *10*, 3261–3266.

(43) Jia, Y.; Li, P.; Gui, X.; Wei, J.; Wang, K.; Zhu, H.; Wu, D.; Zhang, L.; Cao, A.; Xu, Y. *Appl. Phys. Lett.* **2011**, *98*, 1331151–1331154.

(44) Li, R.; iangtao Di,; Yong, Z.; Sun, B.; Li, Q. *J. Mater. Chem. A* **2014**, *2*, 4140–4143.

(45) Yu, L.; Tune, D. D.; Shearer, C. J.; Shapter, J. G. *Solar Energy* **2005**, *118*, 592–599.

(46) Mann, S. A.; de Wild-Scholten, M. J.; Fthenakis, V. M.; van Sark, W. G. J. H. M.; Sinke, W. C. *Prog. Photovolt: Res. Appl.* **2014**, *22*, 1180–1194.

(47) Pintossi, C.; Pagliara, S.; Drera, G.; De Nicola, F.; Castrucci, P.; De Crescenzi, M.; Crivellari, M.; Boscardin, M.; Sangaletti, L. *ACS Appl. Mater. Interfaces* **2015**, *7*, 9436–9444.

(48) Jia, Y.; Cao, A.; Kang, F.; Li, P.; Gui, X.; Zhang, L.; Shi, E.; Wei, J.; Wang, K.; Zhu, H.; Wu, D. *Phys. Chem. Phys.* **2012**, *14*, 83918396.

(49) Cui, K.; Anisimov, A. S.; Chiba, T.; Fujii, S.; Kataura, H.; Nasibulin, A. G.; Chiashi, S.; Kauppinen, E. I.; Maruyama, S. *J. Mater. Chem. A* **2014**, *2*, 11311–11318.

(50) De Nicola, F.; Castrucci, P.; Scarselli, M.; Nanni, F.; Cacciotti, I.; De Crescenzi, M. *Beilstein J. Nanotechnol.* **2015**, *6*, 353–360.

Graphical TOC Entry

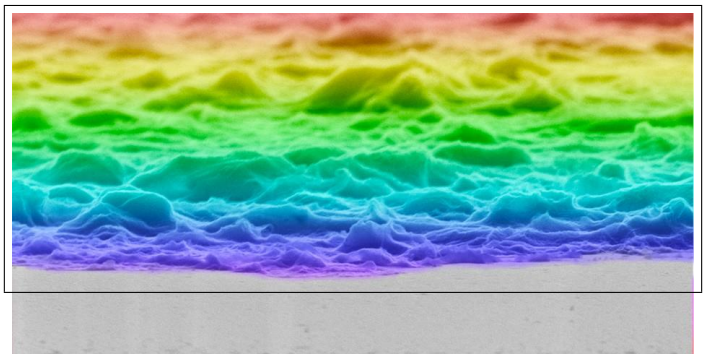

A polychiral SWCNT/Si solar cell.